Supplementary methods

The supplementary methods explains in detail our strategy to explore the parameter space of the Wg receptor interactions based on the observed shapes of decay lengths and amplitudes.

Supplementary methods

Schilling et al.:
A regulatory network of receptors directs range and output of the Wingless morphogen

1 Differential equations describing the Wg-receptor interactions

Our extended model of Wg receptor interactions (sketched in Fig. S5) includes, besides the receptors Arr and Fz2 (summarized in the entity ArrFz2) already present in the core model (Fig. 2), the additional receptor Fz3. Thus the full set of differential equations describing the interaction of Wg with its receptors Arr, Fz2 and Fz3 is given by:

$$\frac{\partial [Wg]}{\partial t} = D_{Wg}\nabla^2[Wg] + k_{0\,Wg}^{DV}(\vec{x}) - k_{Wg}\,[Wg] - rc_{Wg\text{-}ArrFz2} - rc_{Wg\text{-}Fz3}, \tag{S.1}$$

$$\frac{\partial [ArrFz2]}{\partial t} = p_{ArrFz2}^{OE}\cdot k_{0\;ArrFz2} - d_{ArrFz2}^{OE}\cdot k_{Wg\text{-}ArrFz2}^{t}[Wg\text{-}ArrFz2] - k_{ArrFz2}[ArrFz2] - rc_{Wg\text{-}ArrFz2} - k_{Wg\text{-}Fz3\cdot ArrFz2}[Wg\text{-}Fz3][ArrFz2], \tag{S.2}$$

$$\frac{\partial [Wg\text{-}ArrFz2]}{\partial t} = -k_{Wg\text{-}ArrFz2}\,[Wg\text{-}ArrFz2] + rc_{Wg\text{-}ArrFz2} - k_{Fz3\cdot Wg\text{-}ArrFz2}[Fz3][Wg\text{-}ArrFz2], \tag{S.3}$$

$$\frac{\partial [Fz3]}{\partial t} = k_{Fz3}^{pr}[Wg\text{-}ArrFz2] - k_{Fz3}[Fz3] - rc_{Wg\text{-}Fz3} + k_{0\,Fz3}^{OE}, \tag{S.4}$$

$$\frac{\partial [Wg\text{-}Fz3]}{\partial t} = -k_{Wg\text{-}Fz3}\,[Wg\text{-}Fz3] + rc_{Wg\text{-}Fz3}, \tag{S.5}$$

where the reversible complex formation of the ligand Wg (denoted by L) with its receptors $R_1 = ArrFz2$ or $R_2 = Fz3$ is denoted by

$$rc_{L\text{-}R_i} = k_{L\cdot R_i}^{+}[L][R_i] - k_{L\text{-}R_i}^{-}[L\text{-}R_i] \tag{S.6}$$

for $i \in [1, 2]$.
The law of mass conservation implies that ligand and receptor concentration are related by

$$[Wg_T] = [Wg] + [Wg\text{-}ArrFz2] + [Wg\text{-}Fz3], \tag{S.7}$$

$$[ArrFz2_T] = [Wg\text{-}ArrFz2] + [ArrFz2], \tag{S.8}$$

$$[Fz3_T] = [Wg\text{-}Fz3] + [Fz3], \tag{S.9}$$

where the subscript T denotes the total concentration of ligand and receptors.

2 Simplifications

2.1 Neglecting Fz3

The Wg distribution in $fz3^-$ mutant discs is very similar to the corresponding wild-type distribution (Table S1). This observation suggests, that in the wild-type situation Fz3 has only a minor impact on the shaping of the Wg gradient. In a first parameter scan, we therefore reduced the number of free parameters by setting the Fz3 production rate, k_{Fz3}^{pr}, to zero. The equation system eq. (S.1-S.5) simplifies then to

$$\frac{\partial[Wg]}{\partial t} = D_{Wg}\nabla^2[Wg] + k_{0\,Wg}^{DV}(\vec{x}) - k_{Wg}\,[Wg] - rc_{Wg\text{-}ArrFz2}, \tag{S.10}$$

$$\frac{\partial[ArrFz2]}{\partial t} = p_{ArrFz2}^{OE}\cdot k_{0\;ArrFz2} - d_{ArrFz2}^{OE}.k_{Wg\text{-}ArrFz2}^{t}[Wg\text{-}ArrFz2] - k_{ArrFz2}[ArrFz2] - rc_{Wg\text{-}ArrFz2}, \tag{S.11}$$

$$\frac{\partial[Wg\text{-}ArrFz2]}{\partial t} = -k_{Wg\text{-}ArrFz2}\,[Wg\text{-}ArrFz2] + rc_{Wg\text{-}ArrFz2} \tag{S.12}$$

and the mass balance simplifies to

$$[Wg_T] = [Wg] + [Wg\text{-}ArrFz2], \tag{S.13}$$

$$[ArrFz2_T] = [Wg\text{-}ArrFz2] + [ArrFz2]. \tag{S.14}$$

The above equation system describes the Wg-ArrFz2 interactions schematically presented in Fig. 2 of the main text.

2.2 Constant receptor levels in discs lacking endogenous Fz2

In discs lacking all endogenous Fz2, but expressing a $tubFz2$ construct ($fz2^{-}tubFz2$ discs), Wg-induced Fz2 downregulation is purely post-transcriptional.

Remarkably, such discs showed only a very weak Fz2 gradient over the entire disc (Fig. S1). This finding indicates, that the post-transcriptional receptor downregulation seems to have only a small impact on the receptor gradient formation.

This low impact (leading to a nearly constant receptor distribution) might be explained by an excess of unbound receptor compared to the Wg complex: If $[ArrFz2] >> [Wg\text{-}ArrFz2]$ (caused by either an excess of receptor or a high dissociation constant of the receptor complex), then only a small receptor fraction would be post-transcriptionally regulated by Wg binding, subsequent internalization and decay.

Based on our findings in $fz2^{-}tubFz2$ discs, we will therefore make the following simplifications to study the role of receptor upregulation on Wg gradient formation:

$$[R_1] \approx [R_1]_T \equiv [R_1]_{T,0} = const, \qquad k_{L\text{-}R_1}^{t} = 0 \tag{S.15}$$

where we introduced the shorter notation

$$L \equiv Wg,\ R_1 \equiv ArrFz2.$$

Under the assumption of constant receptor levels, we obtain from eq. (S.12) in steady state

$$[L\text{-}R_1] = \frac{1}{k_{L\text{-}R_1}} rc_{L\text{-}R_1} = \frac{1}{k_{L\text{-}R_1}}\left(k_{L\cdot R_1}^{+}[L]\cdot[R_1]_{T,0} - k_{L\text{-}R_1}^{-}[L\text{-}R_1]\right). \tag{S.16}$$

Solving eq. (S.16) for $[L\text{-}R_1]$ we then obtain a linear relationship between receptor-bound (and thus not diffusing) and diffusing Wg:

$$[L\text{-}R_1] = \frac{k_{L\cdot R_1}^{+}[R_1]_{T,0}}{k_{L\text{-}R_1}^{-}+k_{L\text{-}R_1}}[L] = \frac{1}{k_{L\text{-}R_1}}\alpha_e^{L\text{-}R_1}[L], \tag{S.17}$$

where we introduced the effective complex-induced degradation rate

$$\alpha_e^{L\text{-}R_1} = k_{L\text{-}R_1} \frac{k^+_{L\cdot R_1}[R_1]_{T,0}}{k^-_{L\text{-}R_1}+k_{L\text{-}R_1}}. \tag{S.18}$$

Note that $\alpha_e^{L\text{-}R_1}$ does not only depend on kinetic constants, but also linearly on the total mount of receptor. Eq. (S.10) reduces in steady state to

$$k_0^{DV}{}_L(\vec{x}) = -D_L\nabla^2[L](\vec{x}) + k_{Wg}[L] + rc_{L\text{-}R_1}. \tag{S.19}$$

From eq. (S.16-S.17) we obtain

$$rc_{L\text{-}R_1} = \alpha_e^{L\text{-}R_1} \cdot [L], \tag{S.20}$$

which allows us to uncouple eq. (S.19) from the Wg-receptor complex concentration:

$$k_0^{DV}{}_L(\vec{x}) = -D_L\nabla^2[L](\vec{x}) + \alpha_e[L](\vec{x}), \tag{S.21}$$

where

$$\alpha_e = \alpha_e^{L\text{-}R_1} + k_L. \tag{S.22}$$

Eq. (S.21) is a a second order ordinary differential equation (ODE) describing the diffusion of the free ligand Wg (with diffusion constant D_{Wg}) and an "effective degradation rate" α_e, which summarizes the degradation of external, free Wg due to its binding to its receptor, $\alpha_{L\text{-}R_1}$, and its irreversible decay, k_{Wg}.

2.3 One dimensional analytical solution in steady state

With the simplifications (no Fz3,constant receptor levels, no transcriptional receptor regulation) introduced in the previous section, we can find an analytical, one dimensional solution of the Wg distribution (eq. (S.21)).

We consider a constant ligand production in an extended region $[-x_0, 0]$,

$$k_0^{DV}(x) = \frac{s_0}{x_0}\Theta(-x)\Theta(x+x_0). \tag{S.23}$$

Then the Wg distribution outside the production region is given by (Schwank et al., 2011))

$$\begin{aligned} L(x < x_0) &= -f^+(x) \\ L(x > 0) &= -f^-(x), \end{aligned} \tag{S.24}$$

where we defined

$$\begin{aligned} f^\kappa = \frac{s_0}{2x_0\alpha_e}(1 - e^{\kappa x 0/\lambda}) \quad (e^{\kappa x/\lambda}) \\ = C_0 \quad (e^{\kappa x/\lambda}) \end{aligned} \tag{S.25}$$

with $\kappa \in [+,-]$ and the decay length

$$\lambda_e = \sqrt{D/\alpha_e}, \tag{S.26}$$

where α_e is the effective decay rate of the free (external) Wg contribution and λ_e is the corresponding effective decay length. The decay length λ_e corresponds to the distance at which the concentration is reduced by a factor 1/e of C_0. As eq. (S.25) is a purely exponential decay with decay length λ_e, the width of the source, x_0, only impacts the amplitude C_0 of the ligand distribution.

Inside the production region we have

$$L(x \in [-x_0, 0]) = \frac{s_0}{2x_0\alpha_e}(2 - e^{x/\lambda} - e^{-(x+x_0)/\lambda}) \tag{S.27}$$

leading to a flattened ligand profile (Schwank et al., 2011).

3 Relative abundance of free and receptor-bound ligand

The relative abundance of free and receptor-bound ligand Wg over the whole (one dimensional) tissue is given for each component $I_\beta = \int dx \beta(x)$ with $\beta \in [L, L\text{-}R_1]$ by

$$a \equiv I_L = \frac{s_0}{\alpha_e}, \qquad (1-a) \equiv I_{L\text{-}R_1}, \tag{S.28}$$

where we have introduced the fraction of unbound ligand $a \in]0,1[$ and the global concentration normalization

$$I_{L_T} = I_L + I_{L\text{-}R_1} = 1. \tag{S.29}$$

From eq. (S.18) follows then for the receptor-bound Wg fraction

$$I_{L\text{-}R_1} = (1-a) = \frac{\alpha_e^{L\text{-}R_1}}{\alpha_e} \frac{s_0}{k_{L\text{-}R_1}} = a \cdot \frac{\alpha_e^{L\text{-}R_1}}{k_{L\text{-}R_1}}. \tag{S.30}$$

The above equation leads to the following relation between the effective receptor complex decay and the irreversible complex decay rate:

$$\frac{I_{L\text{-}R_1}}{I_L} = \frac{1-a}{a} = \frac{\alpha_e^{L\text{-}R_1}}{k_{L\text{-}R_1}}, \tag{S.31}$$

which leads to

$$k_{L\text{-}R_1} = \frac{a}{1-a} \alpha_e^{L\text{-}R_1}. \tag{S.32}$$

The relative amount of unbound ligand is thus defined by the irreversible decay of the complex and the effective diffusion constant of free Wg:

$$a = \frac{k_{L\text{-}R_1}}{\alpha_e^{L\text{-}R_1} + k_{L\text{-}R_1}}. \tag{S.33}$$

In the most simple model we assume - besides constant receptor levels, no transcriptional receptor regulation and no impact of Fz3 on the Wg distribution - that the Wg decay is dominated by receptor binding and subsequent internalization ($\alpha_{L\text{-}R_1} >> k_L$). Neglecting the irreversible decay of free Wg, we obtain from eq. (S.22)

$$\alpha_e = \alpha_{e,s} = \alpha_e^{L\text{-}R_1}, \tag{S.34}$$

where the subscript "s" denotes here and in the following this most "simple" model. Under this assumption eq. (S.30) simplifies to

$$I_{L\text{-}R_1} = (1-a) = \frac{s_0}{k_{L\text{-}R_1}}. \tag{S.35}$$

Thus in the simple model, the constants α_e and $k_{L\text{-}R_1}$ are fully determined by the relative fractions of unbound and bound Wg, respectively.

For the relationship between total and unbound ligand we obtain with eqs. (S.18) and (S.31)

$$L_T = L + [L\text{-}R_1] = L + \frac{\alpha_e^{L\text{-}R_1}}{k_{L\text{-}R_1}} L = L + \frac{1-a}{a} L = \frac{L}{a}. \tag{S.36}$$

In our Wg stainings, we cannot distinguish between free and receptor-bound Wg and can thus not extract the relative fraction of unbound Wg a from the above equation. But the following section will show, that comparing the peaks of Wg expression in wild-type and receptor-overexpression regions, allows an estimation of this fraction.

4 Constraining the parameter space by comparing the Wg profile in wild-type vs. receptor-overexpressing regions

We model receptor overexpression by increasing the total amount of receptor by a factor $n = p^{OE}_{ArrFz2}$ in the receptor-overexpressing (OE) region

$$[R_1]^{OE}_T = n \cdot [R_1]_{T,0}, \tag{S.37}$$

where $[X]^{OE}$ denotes in the following the concentration of protein X in the receptor-overexpressing region $C = [x1, x2]$: $X^{OE} \equiv [X](x \in C)$. Accordingly, the absence of the superscript OE denotes the corresponding wild-type concentration in the same distance $|x|$ from the Wg source.

In the simple model an n-fold receptor upregulation leads to an n fold larger effective decay rate $\alpha_e^{OE\ L\text{-}R_1} = n\alpha_e^{L\text{-}R_1}$. Accordingly the decay length of free Wg gets reduced by a factor $1/\sqrt{n}$, as with eq. (S.17) we have

$$\lambda^{OE}_{e,s} = \sqrt{\frac{D}{\alpha^{OE\ L\text{-}R_1}}} = \sqrt{\frac{D}{n \cdot \alpha^{L\text{-}R_1}}} = \frac{1}{\sqrt{n}}\lambda_{e,s}, \tag{S.38}$$

where the subscript “s” indicates in the following this most ”simple” relation between wild-type and receptor-overexpression decay lengths.

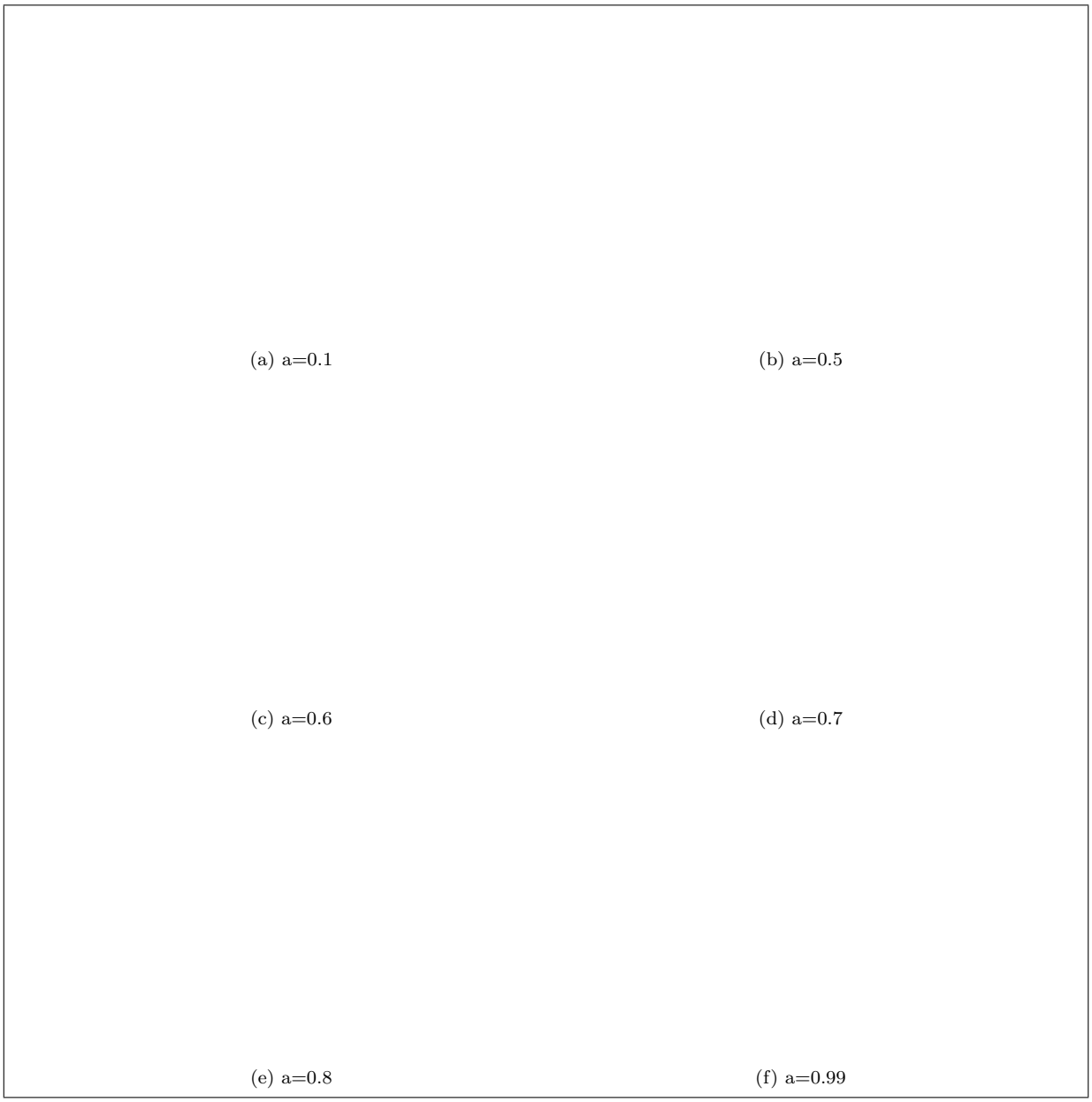

(a) a=0.1 (b) a=0.5

(c) a=0.6 (d) a=0.7

(e) a=0.8 (f) a=0.99

Figure A1: **Comparison of Wg distributions in wild-type (solid lines) and receptor-over expressing regions (x > 0) for dot-dashed lines.**
To mimic Arr overexpressing experiments, we increased the amount of receptor by a factor $n = 2$ for $x > 0$ in graphs with dot-dashed lines. We show the total amount of Wg (black), its free (red) and receptor-bound (green) components and vary the relative amount of free Wg, a. The Wg source is situated between $x_0 = -1/20\ H$ (blue dashed line) and $x = 0$. The decay length of free Wg is set to $\lambda_{Wg} = 22\ \mu$m, the average wild-type decay length measured in discs, where Arr was compartmentally overexpressed. H indicates the half width of the region of interest of length 50 μm.

In Fig. A1 we study the impact of receptor upregulation on the distributions of freely diffusing Wg (red), receptor bound Wg (green) and the total amount of Wg (black) in the simple model. In all plots with dashed lines, we upregulated the amount of receptor by a factor $n = 2$ for $x > 0$. We varied the amount of unbound ligand, a, in between the panels (a) to (f). Solid lines show the distributions in a corresponding wild-type disc. As expected from eq. (S.17), we observe in all scenarios an upregulation of Wg-$ArrFz2$ by a factor n in the overexpression region. The explicit solution for the free ligand in and outside the overexpressing region has been derived in section 4.2 of the supplement of (Schwank et al., 2011). Fig. A1 reveals the dependence of the increase of the amplitude of total Wg (black) in receptor overexpression regions on the relative amount of free ligand a: The higher a, the less the amplitude of the total Wg distribution gets affected by changes in receptor levels. In fact, Schwank et al. have shown (Schwank et al., 2011), that in the most simple model there is a (negative) linear relationship between the fold change ρ of the amplitudes in receptor-overexpressing regions and a.

Comparing the amplitudes of Wg expression in wild-type and receptor-overexpressing compartments (Table S1), we find that they coincide within the measured error bars. Experimentally we cannot distinguish between external free and receptor bound Wg. If the antibody stainings were to show only the freely diffusing Wg (red), then it is very difficult to estimate a from the stainings - wild-type and receptor-overexpression differ for all values of a at the most approx. 25 %. But if the stainings were to reveal the total amount of Wg, Fig.?A1 suggests, that most Wg is freely diffusing ($a > 0.5$): For high values of a (corresponding to a high fraction of freely diffusing, not receptor-bound Wg), wild-type and overexpressing amplitudes differ only slightly and the theoretically predicted difference in the amplitude is in the same range as the variation between biological replica. In the latter case, we can approximate the decay length of free Wg λ_e by the effective decay length λ of all Wg contributions:

$$\lambda_e \approx \lambda. \tag{S.39}$$

Table S1 reveals an agreement between the measurement error with this simple approximation for compartmental Arr overexpression experiments: we find $\lambda^{OE}_{Arr,exp}/\lambda_{Arr,exp} = 0.7 \pm 0.1$, whereas the simple model model predicts $\lambda^{OE}_{Arr,e,s}/\lambda_{Arr,e,s} = \frac{1}{\sqrt{n}} = 0.7$ for an Arr overexpression of roughly a factor $n = 2$.

But in the case of compartmental overexpression of Fz2, the simple model suggests a steeper gradient (smaller λ) in the overexpression situation than actually measured: A Fz2 upregulation of roughly a factor $n = 3.5$ (Table S1) leads to a theoretical value of $\lambda^{OE}_{Fz2,e,s}/\lambda_{Fz2,e,s} = 0.5$, whereas experimentally we find $\lambda^{OE}_{Fz2,exp}/\lambda_{Fz2,exp} = 0.8 \pm 0.1$.

In discs where both receptors Arr and Fz2 were simultaneously upregulated, we observed a similar decrease in the decay length as compared to the upregulation of only one receptor: $\lambda^{OE}_{ArrFz2,exp}/\lambda_{ArrFz,exp} = 0.8 \pm 0.2$. This finding justifies to summarize the effect of the receptors Arr and Fz2 in the entity "ArrFz2" in our modeling approach.

Dropping the assumption of vanishing k_L we obtain

$$\lambda^{OE}_e = \sqrt{\frac{D}{\alpha_e}} = \sqrt{\frac{D}{n \cdot \alpha_e^{L\text{-}R_1} + k_L}}, \tag{S.40}$$

which forecasts a smaller decrease in λ by receptor upregulation than in the naive model. The larger the ratio $k_L/\alpha_e^{L\text{-}R_1}$, the smaller is the expected influence of receptor upregulation on the steepness of the gradient.

5 Parameter estimations

5.1 Kinetic parameters from GFP-tagged Wg in Fluorescence Recovery after Photobleaching (FRAP) experiments

Kicheva et al. (Kicheva et al., 2007) extracted the diffusion constant $D_{Wg\text{-}GFP}$ and the fraction of molecules ψ, that did not recover in the the photo bleached region of interest during the experiment, from the time-dependent recovery profile of Wg-GFP. To do so, they compared a theoretical recovery curve based on on a model, which included Wg production, decay and transport, but did not explicitly take into consideration Wg receptor interactions, with the experimental curves. They varied the fitted parameters $D_{Wg\text{-}GFP}$ and ψ to obtain the best agreement between experimental and theoretical curves and reported

$$D_{Wg\text{-}GFP} = \lambda^2_{Wg\text{-}GFP} \cdot \alpha^{exp} = (0.05 \pm 0.04)\mu\text{m}^2/\text{sec}, \tag{S.41}$$

$$\psi = 0.09 \pm 0.13. \tag{S.42}$$

From the average fluoresence in the receiving territory of Wg e expressing discs they extracted a decay length of

$$\lambda_{Wg\text{-}GFP} = (6 \pm 2)\mu\text{m} \tag{S.43}$$

from which they calculated an effective decay rate of

$$\alpha^{exp} = \frac{D_{Wg\text{-}GFP}}{\lambda^2_{Wg\text{-}GFP}} = (14 \pm 10) \cdot 10^{-4}/\text{sec}. \tag{S.44}$$

In our modeling approach, we summarize the receptors Arr and Fz2 by the receptor entity "ArrFz2". To mimic the average impact of both receptors, we calculated the average wild-type and overexpression (OE) Wg decay lengths in discs, where Arr resp. Fz2 was compartmentally overexpressed (Table S1). In this extracellular Wg antibody stainings, we obtained from a total of eight discs

$$\lambda_{Wg,ArrFz2} = (22 \pm 4)\mu\text{m} \quad \text{and} \quad \lambda^{OE}_{Wg,ArrFz2} = (16 \pm 2)\mu\text{m}. \tag{S.45}$$

Note that this value is significantly larger than the effective decay length measured for GFP-tagged Wg by Kicheva et al. (Kicheva et al., 2007) (eq. S.43). The tagging of Wg by (a relatively large) GFP molecule might hinder its free diffusion, and lead to a smaller decay length of Wg-GFP than of non-tagged Wg.

An alternative explanation for the discrepancy between the decay lengths might be that the theoretical model in Kicheva et al. (Kicheva et al., 2007) did not account for the coupling of diffusion to receptor-mediated uptake and degradation in the fitting procedure of the kinetic parameters. Recently, for the case of DPP-GFP, it has been shown (Zhou et al., 2012) that neglecting this step might lead to an underestimation of extracted diffusion rates and immobile fractions

The measured reduction of the Wg decay length described in the previous subsection is furthermore a strong indicator, that Wg-receptor interactions is indeed shaping the Wg gradient and cannot be neglected in any modeling procedure. Therefore the kinetic parameters of Kicheva et al. (Kicheva et al., 2007) where only used as starting points of our parameter exploration.

5.2 Estimating the relative impact of Wg receptor interaction on gradient formation

The measured change in the decay length under receptor overexpression of Arr and Fz2 (summarized in the following as "ArrFz2"), allows us to extract the relative impact of the complex formation and

subsequent internalization and decay on the shape of the Wg gradient. With eq. (S.38) we obtain

$$0 \leq r_\lambda = \frac{\lambda^2_{Wg,ArrFz2}}{(\lambda^{OE}_{Wg,ArrFz2})^2} \approx \frac{\lambda^2_e}{(\lambda^{OE}_e)^2} = \frac{\alpha^{OE}_e}{\alpha_e} = \frac{n\alpha^{L\text{-}R_1}_e + k_L}{\alpha^{L\text{-}R_1}_e + k_L} = \frac{(n-1)\alpha^{L\text{-}R_1}_e}{\alpha^{L\text{-}R_1}_e + k_L} + 1 = \frac{(n-1)\alpha^{L\text{-}R_1}_e}{\alpha_e} + 1. \tag{S.46}$$

Fom our measurement of the ratio of Wg decay lengths in wild-type and receptor-overexpression situations (Table S1), we obtain

$$r_\lambda = \frac{\lambda^2_{Wg,ArrFz2}}{(\lambda^{OE}_{Wg,ArrFz2})^2} = 1.7 \pm 1.1$$

Assuming an average receptor upregulation of Arr and Fz2 of $n = 3$, we obtain for the relative impact of the Wg - receptor formation an the effective Wg decay constant

$$r_{L\text{-}R_1} = \frac{\alpha^{L\text{-}R_1}_e}{\alpha_e} = \frac{(r_\lambda - 1)}{(n-1)} = 0.3 \pm 0.5 \leq 1. \tag{S.47}$$

Note that for $k_L = 0$, we would expect $r_\lambda = n$ and thus $r_{L\text{-}R_1} = 1$.

5.3 Estimation of the kinetic parameters

Assuming $\alpha_e = \alpha^{exp}$, we can now estimate $\alpha_{L\text{-}R_1}$ from eq. (S.47)

$$\begin{aligned} 0 &\leq \alpha^{L\text{-}R_1}_e = (5 \pm 11) \cdot 10^{-4}/\text{sec} \\ &\leq \alpha^{exp} = (14 \pm 10) \cdot 10^{-4}/\text{sec} \end{aligned} \tag{S.48}$$

Eq. (S.48) can only be an upper bound for the relative impact of the receptor entity "ArrFz2" on the gradient formation. Dropping the assumption of constant receptor levels and taking into account the transcriptional downregulation of the receptors by Wg, $\alpha^{L\text{-}R_1}_{e,f} \equiv k_{L\text{-}R_1} \frac{k^+_{L\cdot R_1}[R_1]}{k^-_{L\text{-}R_1} + k_{L\text{-}R_1}}$ will be significantly smaller in the centre of the disc than far away from the Wg source. The estimation of $\alpha^{L\text{-}R_1}_e$ allows us now to give limits of k_L, too:

$$\begin{aligned} 0 &\leq k_L = \alpha^{exp} - \alpha^{L\text{-}R_1}_e = (9 \pm 14) \cdot 10^{-4}/\text{sec} \\ &\leq \alpha^{exp} = (14 \pm 10) \cdot 10^{-4}/\text{sec} \end{aligned} \tag{S.49}$$

The previous section suggests, that the majority of Wg is unbound. Conservatively assuming $a = 0.5$ we get from eq. (S.32)

$$\begin{aligned} 0 &\leq k_{L\text{-}R_1} = \frac{a}{1-a}\alpha^{L\text{-}R_1}_e = \alpha^{L\text{-}R_1}_e = (5 \pm 11) \cdot 10^{-4}/\text{sec} \\ &\leq \alpha^{exp} = (14 \pm 10) \cdot 10^{-4}/\text{sec} \end{aligned} \tag{S.50}$$

Wu et al (Wu and Nusse, 2002) have measured the binding between Drosophila Wnts and Frizzleds based on a reverse binding assay, in which Wnts are presented on the surface of the cell in the form of type II transmembrane proteins, i.e. with the COOH terminus outside the cells. The cells are then incubated with the ligand-binding domain of Frizzled (the cystein rich domain) tagged with alkaline phosphatase. For the binding of Wg with its receptor Fz2 they measured a dissociation constant of $K_{D\,Wg\,Fz2} = (5.44 \pm 0.26) \cdot 10^{-9}$ Mol[1]. We used this value as an approximation for the dissociation

[1]Note that the corresponding value in (Wu and Nusse, 2002) is wrongly reported as $K_{D\,Wg,\,Fz2} = (5.44 \pm 0.26) \cdot 10^{-8}$ Mol. After personal communication with the authors of (Wu and Nusse, 2002), this error should be corrected in the online version of the article.

constant of Wg hypothetical receptor entity ArrFz2. Whereas this constant was measured in a (three dimensional) biochemical assay, our simulations of Wg receptor interactions are two dimensional. Thus we had to transform between two and three dimensions through the simple expression

$$K_{D\ ArrFz2}^{(3D)} = k_{Wg\cdot ArrFz2}^{+}/k_{Wg-ArrFz2}^{-}, \tag{S.51}$$

where h is the confinement length (Wu et al., 2011). Exploring the parameter space, we varied the confinement length between 1 and 10 micrometers.

5.4 Discussion

Here, we assumed constant receptor levels over the entire disc, justified by the absence of a pronounced gradient in discs lacking endogenous Fz2. In general, this assumption does not hold anymore: the transcriptional downregulation of the receptors Arr and Fz2 by Wg lowers the total amount of receptors up to 50% in the disc center. But under the assumption that only a small Wg fraction gets actually receptor-bound ($[Wg\text{-}ArrFz2] << [Wg]_T$ corresponding to high values of a), this receptor modulation should only have a minor impact on the distribution of total Wg (Table S1).

Thus Fig. A1 suggests that, also in the more general case, most Wg is actually freely diffusing and not bound to its receptors Arr and Fz2. Our findings coincide with the experimental observation of Kicheva et al (Kicheva et al., 2007) that only $(9 \pm 1.3)\%$ of the total amount of Wg are immobile. In our modeling approach this "immobile fraction" corresponds to the receptor-bound Wg fraction.

In the simplified analytical model presented above, we ignored the role of Fz3 on shaping the Wg gradient. Therefore the estimations for the irreversible decay rates of Wg (k_L) and the receptor complex Wg-ArrFz2 ($k_{L\text{-}R_1}$) can only be seen as upper boundaries.

6 Numerical solution of the system of differential equations

6.1 Modeling receptor-misexpression experiments

Modeling loss of receptor experiments

The experimental setup of $fz2^-$ and arr^- mutant cells was modeled by setting the zeroth order production rate of the receptor entity ArrFz2 to zero. Correspondingly, $fz3^-$ mutant cells were modeled by setting the Wg induced production rate of Fz3 to zero. In the latter case the equation system eq. (S.1-S.5) reduces to the system of partial and differential equations describing the simplified network of Wg/ArrFz2 interactions depicted in Fig. 2 of the main text and given in eq. (S.10-S.14).

Modeling receptor-overexpressing experiments

Based on our experimental observation that under the regime of the *tubulin*α1 promoter the maximal receptor levels of Arr and Fz2 were enhanced by a factor 2 to4 (Fig. 1F, 1R, Table S1), we increased the production rate of the receptor entity ArrFz2 by a factor $n = 3$ in receptor-overexpressing cells.

Our analysis of receptor levels in discs, where Arr resp. Fz2 receptor levels were overexpressed (Fig. 1), revealed that in both cases the slope in receptor-overexpressing discs was slightly reduced (Fig. 1, Table S1). But in discs expressing the *tubFz2* construct, but lacking all endogenous Fz2, the Fz2 expression gradient got weakened (Fig. S1).

This experimental finding suggests, that only the wild-type fraction of the receptor gets transcriptionally downregulated, whereas post-transcriptional downregulation seems to have a minor impact on the receptor gradient formation (Fig. S1). We incorporate these experimental observations by introducing a dampening factor d_{ArrFz2}^{OE} of the Wg signaling mediated decay rate of ArrFz2 (eq. (S.2)). Whereas this

factor is assumed to equal 1 in wild-type cells, we varied it between 0 and 1 in receptor-overexpressing cells.

To take into consideration the transcriptional upregulation of Fz3 in Fz3 overexpressing discs, we introduced an additional zeroth order, thus Wg independent, Fz3 production term $k_{0\,Fz3}^{OE}$. In the wild-type simulation runs, this additional Fz3 production term was set to 0.

6.2 Modeling diffusion on a mesh generated by a vertex model

Extending our Wg receptor interaction model to two dimensions, we wanted to numerically solve the corresponding Wg diffusion equation on a mesh, which resembled the cell shapes of the apical side of a *Drosophila* wing disc. The vertex model fulfills this requirement: It describes cells and their contact surfaces as as a graph of connected vertices with positions defined by the local minimum of an energy function. This energy functions describes the mechano-elastic properties of the tissue(Farhadifar et al., 2007) characterized by the interplay of the line tension, the term of the energy function proportional to the edge length between two connected vertices, and the cell's contractility. We parametrized the relative impact of the line tension on the normalized energy function with $\overline{\Lambda} = 0.12$ and the relative impact of the contractility with $\overline{\Gamma} = 0.04$ ('case I' of (Farhadifar et al., 2007)). These parameters were chosen such, that the resulting network of polygons resembles the network topology of the apical cells of the wing disc. Using these polygons as local control volumes, we discretized the diffusion of Wg by the Finite Volume Method.

Implementing compartment boundaries

To mimic compartmental receptor overexpression experiments, we modeled the observed sharp anterio-posterior compartment boundary (Farhadifar et al., 2007) by increasing the $\overline{\Lambda}$ by a factor 2.5 for all edges shared between an anterior and posterior cell. In analogy, we implemented the increased line tension at the dorsoventral compartment boundary (Dahmann et al., 2011) by increasing the line tension term between Wg producing cells and all other cells (Dahmann et al., 2011) by the same factor.

Modeling growth

In simulation runs, which included the growth of the disc, we had to accurately compute the two-dimensional diffusion of the Wg protein on a geometry that is itself constantly changing. We achieved this by alternating the mechanical relaxation/growth computations of the cellular vertex model (Farhadifar et al., 2007) with the numerical solution of the coupled system of ordinary and partial differential equations given in eq. (S.1.-S.9) within each cell (as described in the supplement of (Schilling et al., 2011)). This modeling approach allowed us to simulate compartmental receptor overexpression experiments with cellular resolution on a cell topology which resembles an actual wing disc (Farhadifar et al., 2007). Movies 1 and 2 show the Wg resp. ArrFz2 concentrations of an exemplary simulation run of a growing wing disc.

7 Parameter exploration based on the shapes of Wg and receptor distributions

The analytical solution of the simplified one-dimensional model suggested that the majority of Wg is freely diffusing. It allowed us furthermore to define upper boundaries for the Wg and Wg-ArrFz2 decay constants based on the measured effective Wg decay constant. We approximated the dissociation constant of the complexes Wg-ArrFz2 and Wg-Fz3 by the measured dissociation constant of Wg-DFz2. In order to set the remaining parameters of the full two dimensional numerical model, we transformed the

above systems of equations into its non-dimensional form (Dillon and Othmer, 1999; Reeves et al., 2005). This procedure leads to dimensionless groups of the kinetic parameters, which we varied up to three orders of magnitude within physiological meaningful ranges. To explore the parameter space, we varied one parameter at a time, whilst fixing all remaining parameters. A total of roughly 10'000 parameter sets was scanned. A valid parameter entering eqs. (S.1-S.9) set had to qualitatively reproduce the shape of Wg and receptor distributions in the wild-type and receptor mutant situations as parameterized in Table S1. Remarkably, the parameter exploration suggested that the complex formed by Wg and Fz3 might be more stable than the corresponding Wg-ArrFz2 complex, confirming the Wg stabilizing role of Fz3. Furthermore, only relatively high Wg diffusion constants ($D = 4\ \mu\text{m/sec}^2$ in the exemplary parameter set displayed in Table S2 below), allowed us to describe our data. This value is roughly 80 times larger than the effective diffusion coefficient of GFP-tagged Wg reported by Kicheva et. al. (Kicheva et al., 2007). However, Kicheva et al. neglected an explicit modeling of the coupling of diffusion to receptor-mediated uptake in their fitting procedure, an approach that might lead to an underestimation of the extracted diffusion coefficient (section 5.1, (Zhou et al., 2012)).

Table S2: **Characteristic units, geometry and parameters of the Wg-receptor model**

	Value	Annotation	Source
Characteristic units			
length	$L = 1\mu$m	micrometer	
time	$T = 1$ h	hour	
concentration	$U = 1000$ molecules/cell		
Geometry			
l	1 μm	confinement region of length l perpendicular to cell membrane	(Wu et al., 2011), (Dustin et al., 2001)
A_{cell}	5.4 μm^2	average wing disc cell area	(Farhadifar et al., 2007)
Parameters			
Zeroth order production	$k_0 = 67.32$ U/h		
$k_{0\,Wg}^{DV}$	k_0	production at DV boundary	(Kicheva et al., 2007)
$k_{0\,ArrFz2}$	$10^{-3} \cdot k_0$	wt production rate of ArrFz2	
n	3	average receptor upregulation	Table S1
$k_{0\,ArrFz2}^{OE}$	$n \cdot 10^{-3} \cdot k_0$	OE production rate of ArrFz2	
$k_{0\,Fz3}^{OE}$	$10^{-2} \cdot k_0$	OE production rate of Fz3	
First order production	$k_1 = 2.52$/h		
k_{Fz3}^{pr}	$0.2 \cdot k_1$	Wg signaling induced Fz3 prod.	
First order decay			
k_{Wg}	k_1	Wg decay	(Kicheva et al., 2007)
k_{ArrFz2}	k_1	ArrFz2 decay	
k_{ArrFz2}^{t}	1.2 k_1	transcriptional and translational repression of ArrFz2 by Wg-ArrFz2	
d_{ArrFz2}^{OE}	1/2	dampening factor	section 6.1
$k_{ArrFz2,2}^{OE}$	$d_{ArrFz2}^{OE} \cdot k_{ArrFz2}^{t}$	Wg signaling induced repression in receptor OE cells	
k_{Fz3}	$2 \cdot k_1$		
$k_{Wg\text{-}ArrFz2}$	$0.8 \cdot k_1$		
$k_{Wg\text{-}Fz3}$	$0.2 \cdot k_1$	Wg-Fz3 is more stable than Wg-ArrFz2	
Dissociation const. (3D)			
$K_{D,Wg\text{-}DFz2}^{3D}$	$5.4 \cdot 10^{-9}$ M	$k_{Wg-DFz2}^{-}/k_{Wg-DFz2}^{+}$	(Wu and Nusse, 2002),
$K_{D,Wg\text{-}ArrFz2}^{3D}$	$5.4 \cdot 10^{-9}$ M	approximation of dissociation constant	section 5.3
Dissociation const. (2D)			
l	$l = 1\ \mu$ m	l: confinement length	
$K_{D,Wg\text{-}ArrFz2}^{2D}$	$l \cdot K_{D,Wg\text{-}ArrFz2}^{3D}$ = 3.2 molecules/μm^2 = 17.8 molecules/A_{cell} = 0.0178 U		(Wu et al., 2011)
Equilibrium const. (2D)			
$K_{Wg\text{-}ArrFz2}$	≈ 56/U	inverse of dissociation constant	
$K_{Wg\text{-}Fz3}$	≈ 56/U		
Second order decay	k2 $[1/(T \cdot U)]$		
$k_{Fz3 \cdot Wg\text{-}ArrFz2}$	$k_2 = k_1 \cdot K_{Wg\text{-}ArrFz2}$	Fz3 introduced repression of Wg-ArrFz2	
$k_{Wg\text{-}Fz3 \cdot ArrFz2}$	k_2	Wg-Fz3 introduced repression of ArrFz2	
Diffusion const.			
D_{Wg}	4 μm^2/s=14400 μm^2/h	diffusion constant of free Wg	

References

Dahmann, C., Oates, A. C. and Brand, M. (2011). Boundary formation and maintenance in tissue development. *Nature Reviews Genetics* **12**, 43–55.

Dustin, M. L., Bromley, S. K., Davis, M. M. and Zhu, C. (2001). Identification of self through two-dimensional chemistry and synapses. *Annual review of cell and developmental biology* **17**, 133–157.

Farhadifar, R., Röper, J.-C., Aigouy, B., Eaton, S. and Jülicher, F. (2007). The influence of cell mechanics, cell-cell interactions, and proliferation on epithelial packing. *Current Biology* **17**, 2095–2104.

Kicheva, A., Pantazis, P., Bollenbach, T., Kalaidzidis, Y., Bittig, T., Jülicher, F. and González-Gaitán, M. (2007). Kinetics of morphogen gradient formation. *Science (New York, NY)* **315**, 521–525.

Schilling, S., Willecke, M., Aegerter-Wilmsen, T., Cirpka, O. A., Basler, K. and von Mering, C. (2011). Cell-sorting at the A/P boundary in the Drosophila wing primordium: a computational model to consolidate observed non-local effects of Hh signaling. *PLoS Computational Biology* **7**, e1002025.

Schwank, G., Dalessi, S., Yang, S.-F., Yagi, R., de Lachapelle, A. M., Affolter, M., Bergmann, S. and Basler, K. (2011). Formation of the long range dpp morphogen gradient. *PLoS Biology* **9**, e1001111.

Wu, C.-h. and Nusse, R. (2002). Ligand receptor interactions in the Wnt signaling pathway in Drosophila. *The Journal of biological chemistry* **277**, 41762–41769.

Wu, Y., Vendome, J., Shapiro, L., Ben-Shaul, A. and Honig, B. (2011). Transforming binding affinities from three dimensions to two with application to cadherin clustering. *Nature* **475**, 510–513.

Zhou, S., Lo, W.-C., Suhalim, J. L., Digman, M. A., Gratton, E., Nie, Q. and Lander, A. D. (2012). Free extracellular diffusion creates the Dpp morphogen gradient of the Drosophila wing disc. *Current biology : CB* **22**, 668–675.

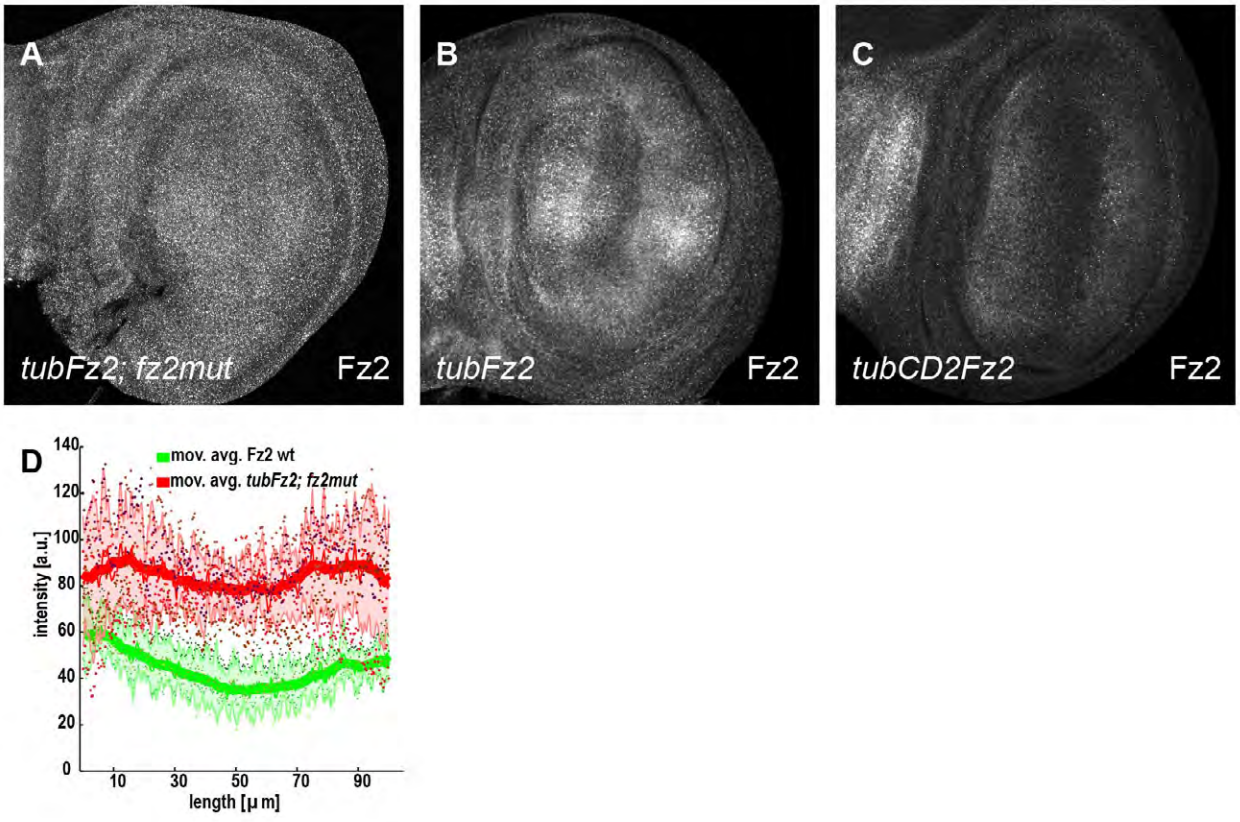

Figure S1: Fz2 gradient in *tubFz2* discs is maintained by endogenous Fz2 expression

Panel (A) shows a disc expressing the *tubFz2* transgene, but lacking all endogenous Fz2, thereby showing a weaker gradient of Fz2 expression. Panel (B) depicts a *tubFz2* disc with endogenous Fz2, while panel (C) shows a wild-type control. In (D) a maximum intensity projection of the receptor distributions of four wild-type and five *tubFz2*, *fz2*$^{-}$ discs are shown.

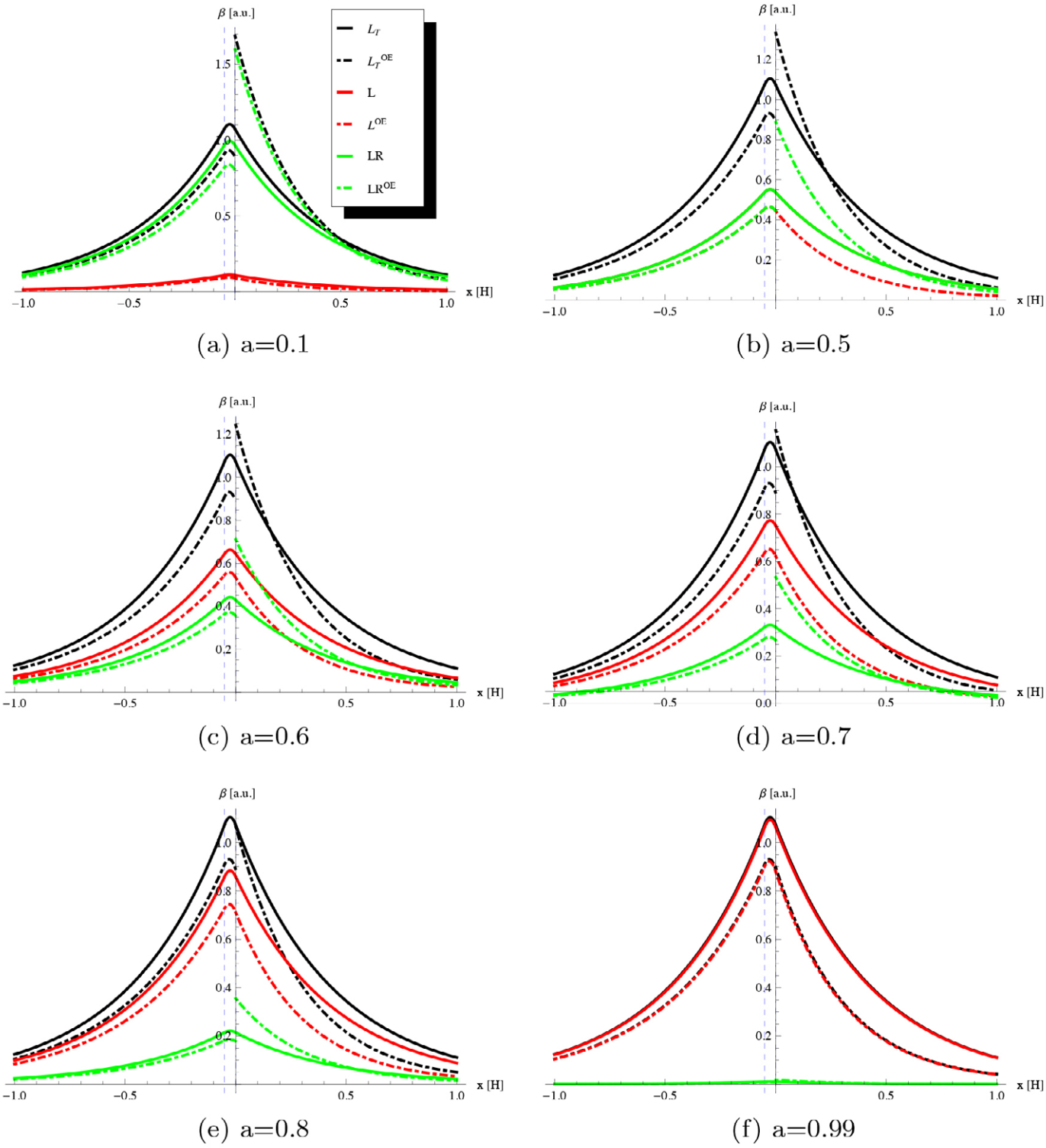

Figure S2: Comparison of Wg distributions in wild-type (x<0, solid lines) and receptor-overexpressing regions (x>0, dot-dashed lines) in a simplified model

We solved a simplified model of Wg-receptor interactions analytically (neglecting Fz3, no transcriptional receptor downregulation, no decay of unbound Wg)**.** To mimic Arr overexpressing experiments, we increased the amount of receptor by a factor n=2 for x>0 in graphs with dot-dashed lines. We show the total Wg (black), its free (red) and receptor-bound (green) components and vary the relative amount of free Wg, *a*. The Wg source is situated between $x_0 = -1/20 \times H$ (blue dashed line) and $x = 0$. The decay length of Wg is set to $l_{Wg} = 21\,\mu m$, the average wild-type decay length measured in discs, where Arr was compartmentally overexpressed. H indicates the half width of the region of interest of length $50\,\mu m$. Note the dependence of the increase in the amplitude of total Wg in the receptor-overexpression region on *a*.

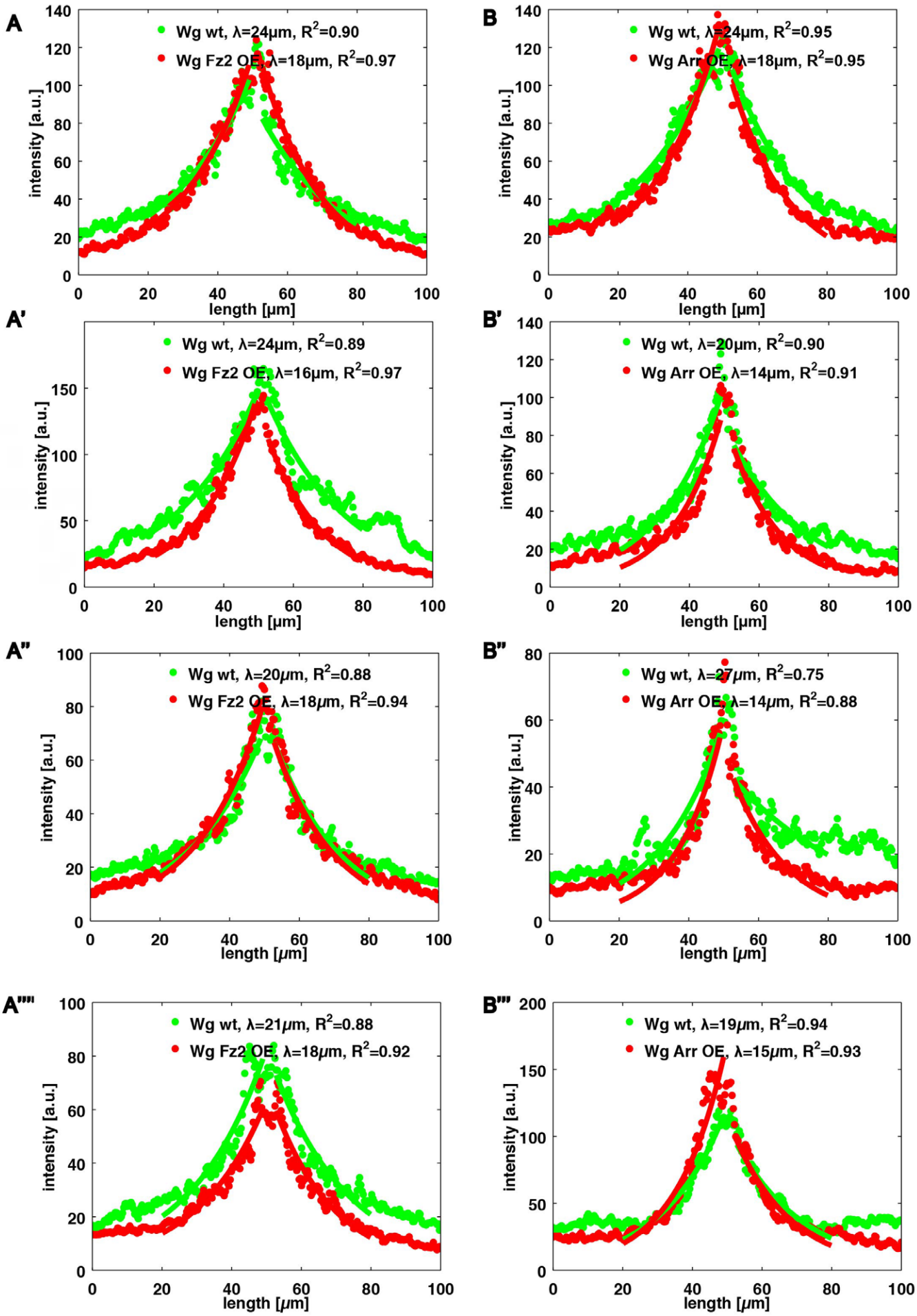
A
Wg wt, λ=24μm, R²=0.90
Wg Fz2 OE, λ=18μm, R²=0.97
intensity [a.u.]
length [μm]
B
Wg wt, λ=24μm, R²=0.95
Wg Arr OE, λ=18μm, R²=0.95
intensity [a.u.]
length [μm]
A'
Wg wt, λ=24μm, R²=0.89
Wg Fz2 OE, λ=16μm, R²=0.97
intensity [a.u.]
length [μm]
B'
Wg wt, λ=20μm, R²=0.90
Wg Arr OE, λ=14μm, R²=0.91
intensity [a.u.]
length [μm]
A''
Wg wt, λ=20μm, R²=0.88
Wg Fz2 OE, λ=18μm, R²=0.94
intensity [a.u.]
length [μm]
B''
Wg wt, λ=27μm, R²=0.75
Wg Arr OE, λ=14μm, R²=0.88
intensity [a.u.]
length [μm]
A''''
Wg wt, λ=21μm, R²=0.88
Wg Fz2 OE, λ=18μm, R²=0.92
intensity [a.u.]
length [μm]
B''''
Wg wt, λ=19μm, R²=0.94
Wg Arr OE, λ=15μm, R²=0.93
intensity [a.u.]
length [μm]

Figure S3: Narrowing of the extracellular Wg distribution upon receptor overexpression

Panels A-A''' show the extracellular Wg distribution in the posterior (displayed in red) and anterior (displayed in green) compartment of a single disc. In the posterior compartment, a *tubArr* construct was expressed by flipping out a *CD2* stop cassette via *hhGal4 UAS-Flp*. Panels B-B''' show the same, but here a *tubFz2* construct was used. We display the mean decay length λ and R^2 for the wild-type and receptor-overexpressing compartment of each disc. Fitting procedure as described in "Materials and Methods" section.

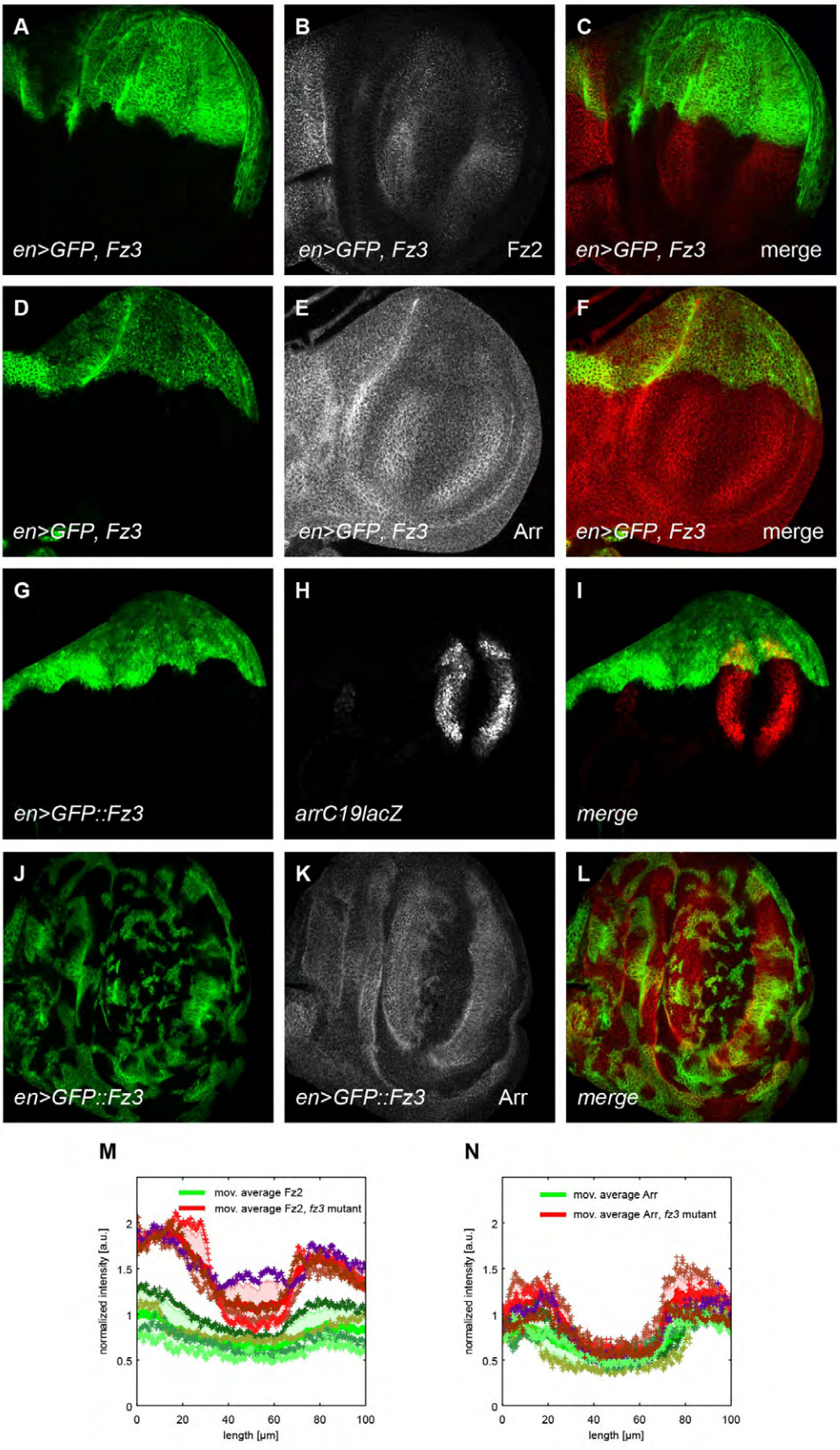

Figure S4: Fz3 downregulates Arr and Fz2 posttranscriptionally

Fz3 overexpression (green in A, D, G) in the P compartment reduces Fz2 levels (grey in B) and Arr levels (grey in E), but does not reduce *ArrC19* expression (G-I). In contrast, Arr protein levels are higher in Fz3 overexpressing clones away from the Wg source (J-L). Intensity profiles of Fz2 gradients (M) and Arr gradients (N) in *fz3* mutant (red) and wild-type wing discs (green). Note the higher intensity profiles of Fz2 and Arr in the *fz3* mutant wing disc.

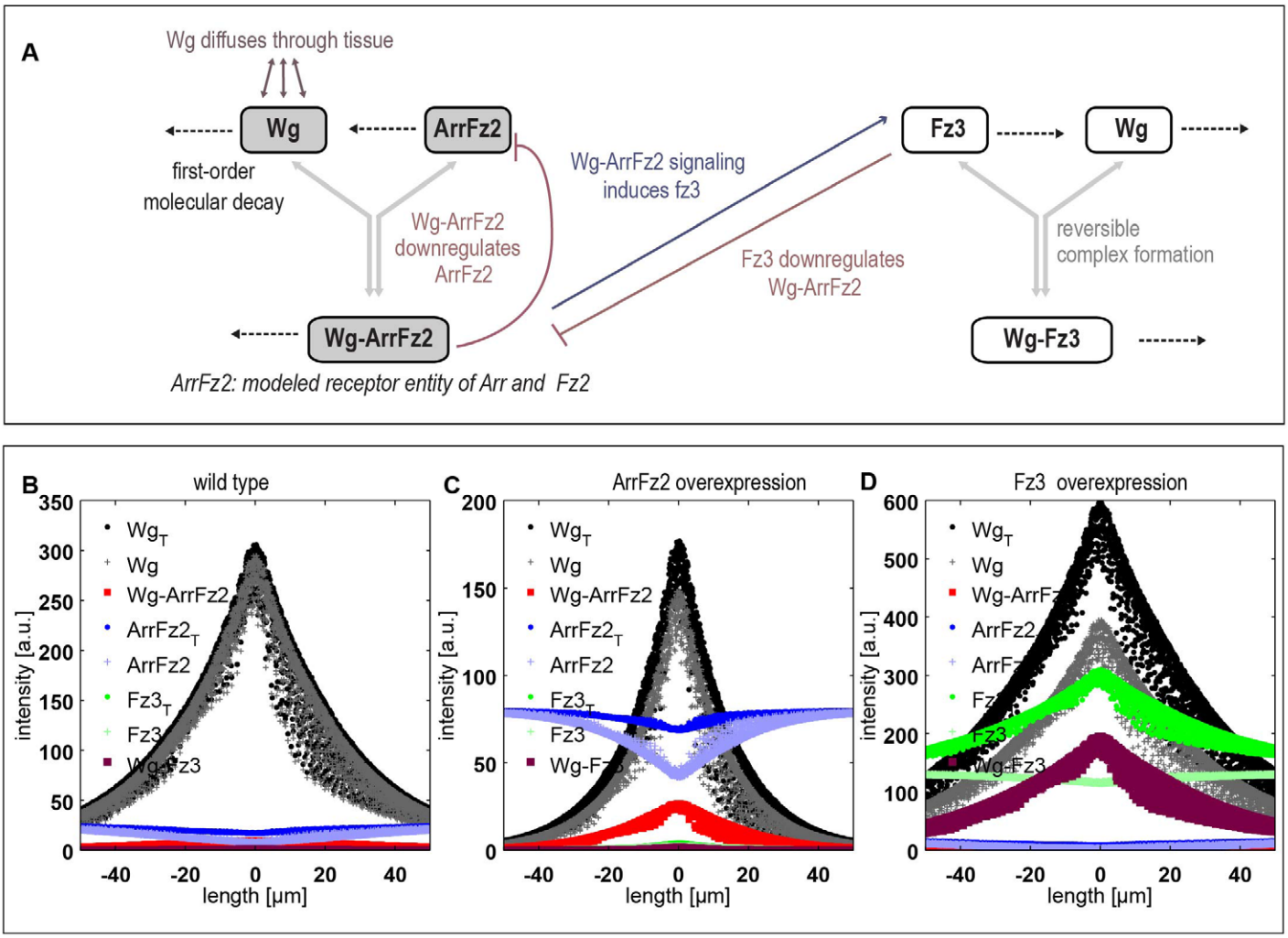

Figure S5: Model describing Wg signaling as the interplay of the two reversibly forming complexes, Wg-ArrFz2 and Wg-Fz3

In our extension of the original model (Fig. 2) the production of a second receptor Fz3 depends on Wg signaling (as modeled by the presence of the Wg-ArrFz2 complex). Fz3 itself attenuates Arr and Fz2 only in interaction with Wg. (B-D) Exemplary simulation run of full model with wild-type (B), ArrFz2 overexpression (C) Fz3 overexpression parameter sets (Table S2 of the Supplementary methods). Projection of the concentrations of all simulated players on the anterioposterior axis.

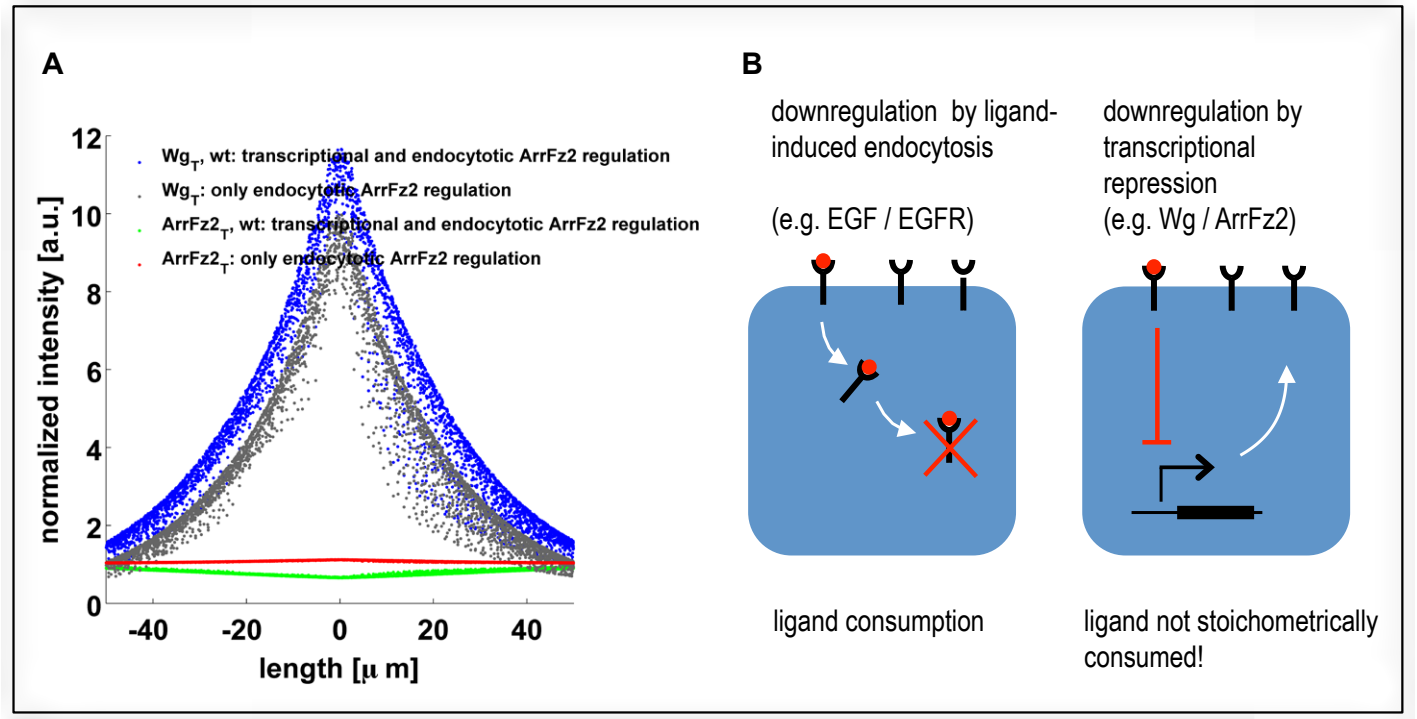

Figure S6: Transcriptional receptor regulation leads to broader Wg distribution

(A) We modeled purely endocytotic receptor downregulation (Wg distribution in grey, receptor distribution in red) by setting the Wg signaling induced transcriptional decay rate $k^t_{Wg\text{-}ArrFz2}$ in eq. (S.2) to 0. Note that with transcriptional receptor regulation, we observe a slightly broader Wg distribution and higher Wg amplitude (blue). (B) Schematic view of receptor downregulation by ligand-induced endocytosis vs. transcriptional repression.

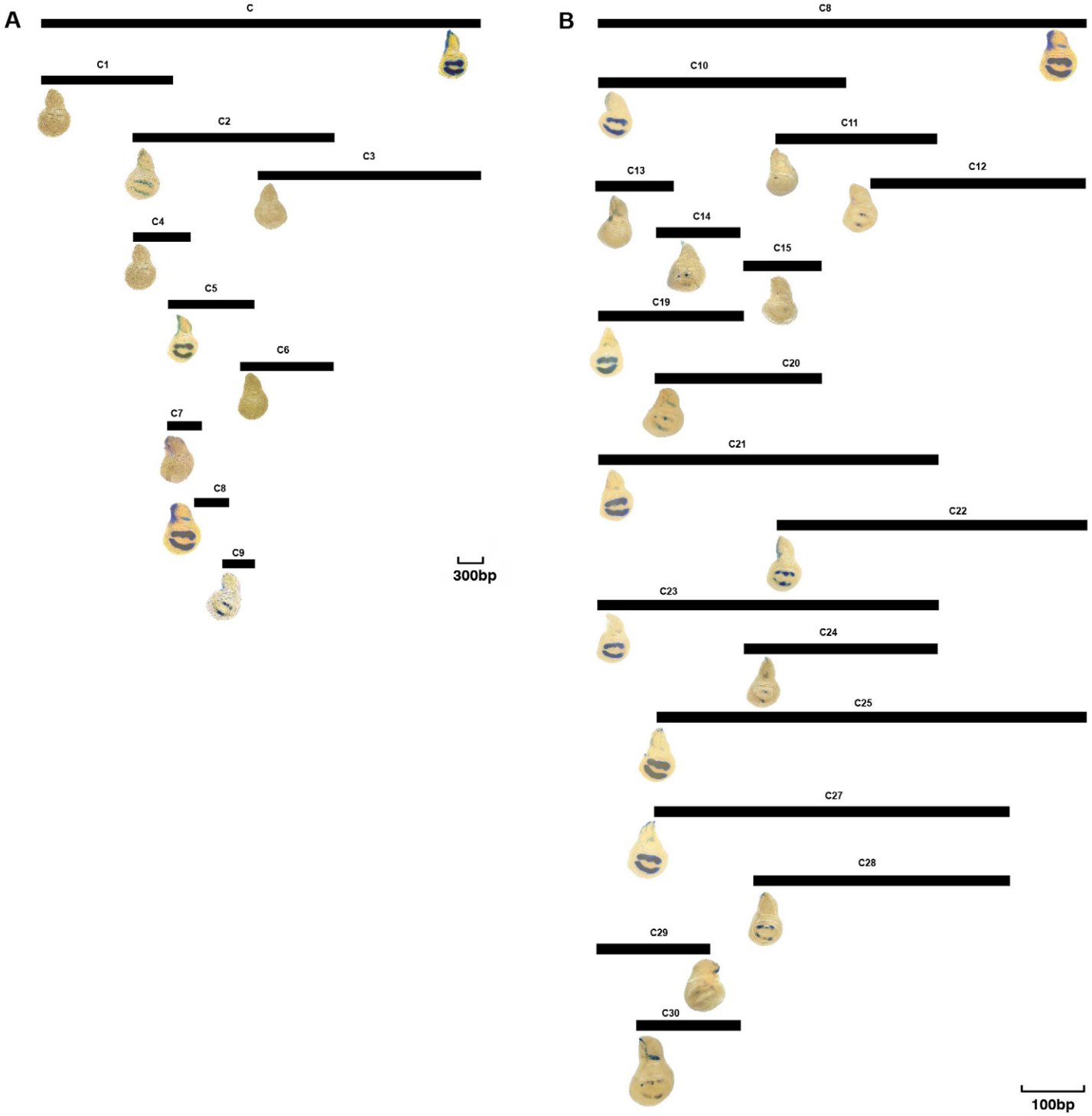

Figure S7: Dissection of the arr regulatory region

Panel (A) depicts the different genomic fragments from the *arr* regulatory region, which were cloned into a *lacZ* reporter vector and integrated into the same landing site on the second chromosome. Expression of *lacZ* in wing discs from third instar larvae is monitored by standard X-Gal staining assays. Dissection of the *arrC* enhancer results in *arrC8* and further narrowing down of *arrC8* yields the minimal enhancer *arrC19* (B).

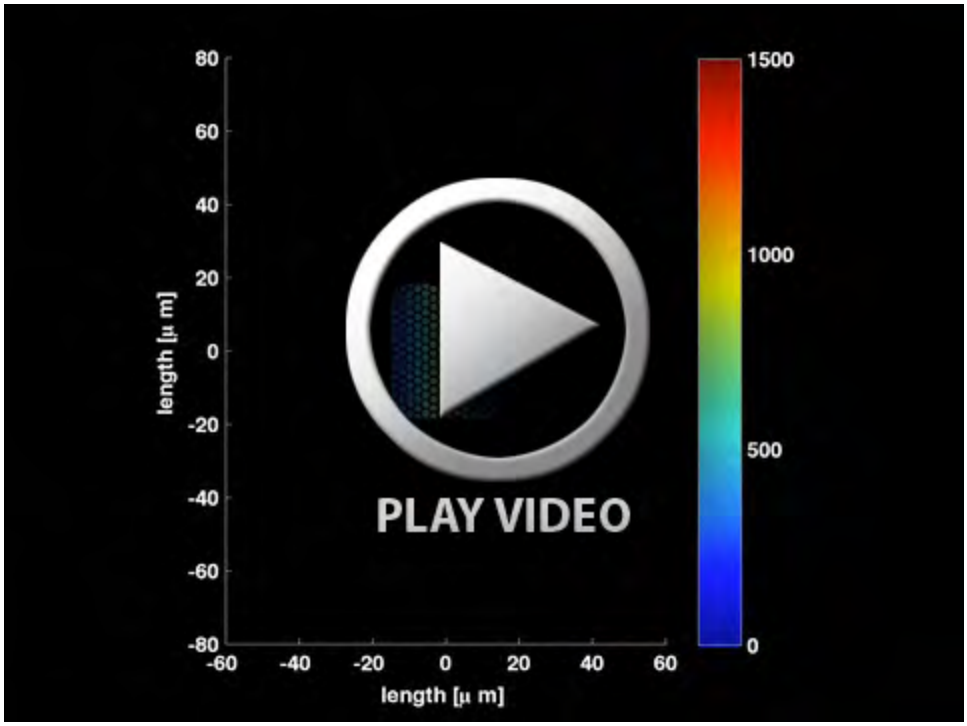

Movie 1: Total Wg distribution on a growing disc
We interchanged the simulation of the growth of the disc with the solution of the differential equations on the ever-changing cell topology (see Supplementary methods) for an exemplary parameter set. Note the increase in the Wg amplitude during the growth of the disc.

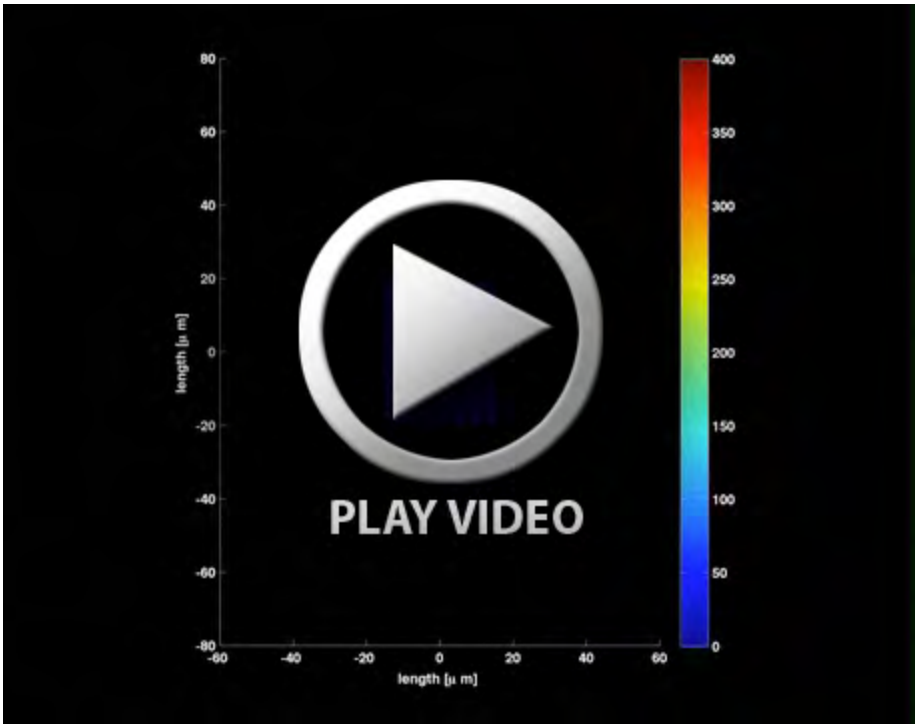

Movie 2: Total Arrow distribution on a growing disc

Table S1, Schilling et al.

Wg distributions: Exponential fits

Exponential fit of form $y = y_0 \cdot \exp(-x/\lambda)$, where
λ, y_0, R^2: mean decay length, mean amplitude and mean correlation coefficient of N discs

	λ [µm]	y_0 [a.u.]	R^2	N
Experiment				
Wg, wt	22 ± 2	113 ± 39	0.90	4
Wg, *tubFz2*	18 ± 3	107 ± 34	0.96	4
Wg, wt	21± 5	112 ± 26	0.89	4
Wg, *tubArr*	15 ± 2	117 ± 32	0.93	4
Wg, wt	35 ± 11	109 ± 42	0.74	9
Wg, *tubArrtubFz2*	26 ± 7	119 ± 52	0.81	9
Wg, wt	19 ± 11	66 ± 15	0.92	2
Wg, *tub Fz2; fz2mut*	18 ±4	72 ± 17	0.87	8
Wg, wt	23 ± 9	93 ± 20	0.85	4
Wg, *fz3*$^-$	21 ± 5	112 ± 16	0.81	4
Wg, wt	29 ± 5	39 ± 5	0.85	4
Wg, Fz3 OE	43 ± 13	81 ± 24	0.80	4
Simulation				
Wg, wt	23 ± 2	275 ± 41	0.90	10
Wg, ArrFz2 OE	14 ± 1	198 ± 30	0.89	10
Wg, Fz3 OE	38 ± 8	647 ± 86	0.87	10

Compartmental receptor mixexpression: Ratio of Wg amplitudes and decay lengths

Ratio of Wg amplitudes and decay lengths of the receptor overexpressing (OE) and wild type compartment are calculated for each disc, shown mean and standard deviation of N discs
p: p-value of hypothesis that amplitudes and decay length remain unchanged under receptor OE

	y_0^{OE}/y_0	p (y_0^{OE}/y_0-1)	$\lvert\lambda^{OE}/\lambda\rvert$	p (λ^{OE}/λ-1)	N
Experiment					
Wg, *tubFz2* / Wg, wt	1.0 ±0.1	0.42	0.8 ±0.1	0.0004	4
Wg, *tubArr* / Wg, wt	1.1 ±0.2	0.57	0.7 ±0.1	0.0002	4
Wg, *tubArrtubFz2* / Wg, wt	1.3 ± 0.3	0.30	0.8 ± 0.2	0.0020	9
Wg, Fz3OE / Wg ,wt	2.1 ± 0.7	0.05	1.3 ± 0.2	0.0390	4
Simulation					
Wg, ArrFz2 OE / Wg, wt	0.7 ± 0.1	$4 \cdot 10^{-8}$	0.61 ± 0.03	$2 \cdot 10^{-9}$	10
Wg, Fz3 / Wg, wt	2.4 ± 0.3	$6 \cdot 10^{-8}$	1.7 ± 0.3	$2 \cdot 10^{-5}$	10

Recptor distributions: Second order polynomial fit

Second order polynomial fit of form $y = ax^2+bx+c$; a b,c are the mean fit coefficients of N discs

	$a \cdot 10^5$ [a.u./µm2]	b [a.u./µm]	c [a.u.]	R^2	N
Experiment					
Fz2, wt	18 ± 4	-0.019 ± 0.004	1.1 ± 0.2	0.62	4
Fz2, *tubFz2*	34 ± 15	-0.036 ± 0.013	3.8 ± 0.4	0.48	4
Fz2, wt	18 ± 8	-0.018 ± 0.008	1.1 ± 0.3	0.78	4
Fz2, *fz3*$^-$	51 ± 16	-0.055 ± 0.018	2.6 ± 0.4	0.77	4
tubFz2; fz2mut	15 ± 22	-0.015 ± 0.021	1.7 ± 0.6	0.40	5
Arr, wt	27 ± 7	-0.025 ± 0.006	1.1 ± 0.3	0.84	4
Arr, *tubArr*	32 ± 17	-0.032 ± 0.015	2.4 ± 0.3	0.67	4
Arr, wt	33 ± 3	-0.031 ± 0.004	1.2 ± 0.2	0.80	4
Arr, *fz3*$^-$	49 ± 12	-0.048 ± 0.011	1.8 ± 0.3	0.79	4
Simulation					
ArrFz2, wt	18 ± 2	-0.00011 ± 0.00016	0.7 ± 0.0	0.85	10
ArrFz2, OE	42 ± 4	0.00019 ± 0.00014	2.7 ± 0.1	0.76	10

Table S1: Quantification of wild-type and receptor-misexpression Wg and receptor distributions in experiment and simulation

Experiment: We display the mean correlation coefficient $R^2 = \sum_{i=1}^{N} R_i^2$ of *N* measurements.
For Wg distributions, we display the mean of the absolute value of the decay length and amplitude. For receptor distributions we display the mean fit coefficients to a second order polynomial. In discs where the receptor misexpression was compartmental, we calculated furthermore the change in Wg amplitudes and decay length and displayed the mean of N measurements.
Simulation: Based on the parameter set given in Table S2 of the Supplementary methods, simulations were run on 10 different network topologies, containing between 4000 and 9000 cells. For each network topology, we projected the simulated concentration of total Wg and ArrFz2 of each cell on the anterio-posterior axis (example projection is shown in Figure 4). The extraction of the decay lengths followed the experimental fitting procedure described in the “Materials and Methods” section. All errors are standard deviations.